Trigonometric Approximation of Radar Cross Section: A Quick Survey

Daniel Topa
ERT Corp

April 15, 2020

Abstract

The challenge is to expand the capability of the AFCAP dashboard by offering a refined representation of the radar cross section. Currently, the radar cross section is a constant. What is the best way to include a more realistic radar cross section computed from simulation? One avenue discussed herein is to approximate the radar cross section as trigonometric polynomial. A mathematical summary of the approximation process follows, concluding with a numeric example.

1 Foundation

1.1 Problem statement

One method to enhance probability of detection in the AFCAP dashboard is to improve the fidelity of the radar cross section (RCS). Currently, the radar cross section is a the scalar value, a constant.[1] What is the best way to include a more detailed RCS computed from a numerical code such as Mercury MoM?

1.2 Simulation

To start the exploration, an elementary aircraft model, the Sciacca airframe, shown in figure 1.2, was created for use in Mercury MoM. The simplicity of

[1] As seen in §4.6, the offset term dominates in the least squares approximation sequence.

the model evinces the resolution of the radar frequencies of interest: 3 Mhz – 30 MHz, corresponding to wavelengths of 100 m – 10 m.

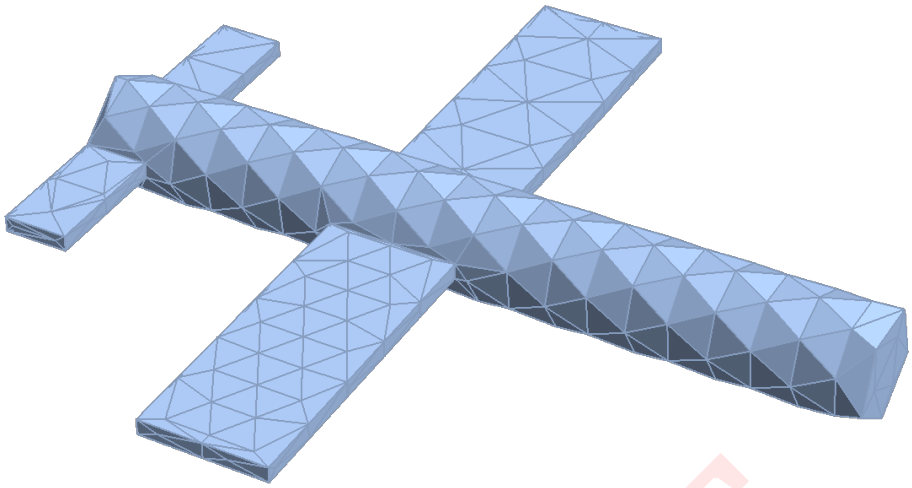

Figure 1.1: Sciacca airframe for simplistic RCS modelling.

1.3 Coordinate system

The coordinate system is based upon the aircraft principal axes. The yaw angle is α, the pitch angle β as shown in table 1.1. The pitch is also referred to as elevation, and will be fixed at 30°.

1.4 Simulation results

Figure 1.4 is a graphical depiction of the RCS computations from the Mercury MoM simulation for the Sciacca airframe. The simulation is based on the input frequency ν in MHz and was constrained to the integer sequence $\{3, 4, \ldots, 30\}$.

Physical intuition is aided by showing the corresponding wavelength range. The linear scale of the frequency (ν) is connected to the hyperbolic scale of the wavelength (λ) using:

$$\lambda\nu = c. \tag{1.1}$$

Table 1.2 shows the radar cross section for the aircraft at four different frequencies corresponding to wavelengths of 11, 50, 75, and, 100 meters. These individual curves are the targets of the ensuing Fourier decomposition.

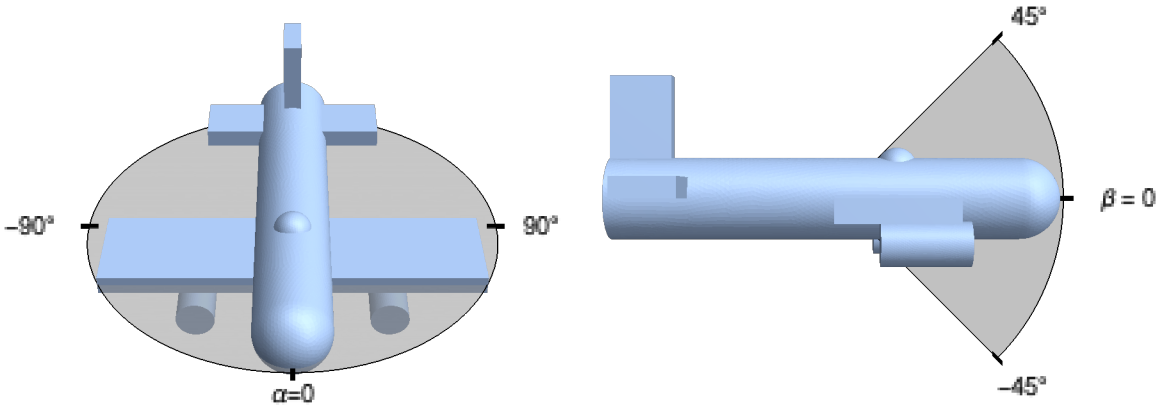

Table 1.1: The aircraft principle angles showing yaw (α) and pitch (β).

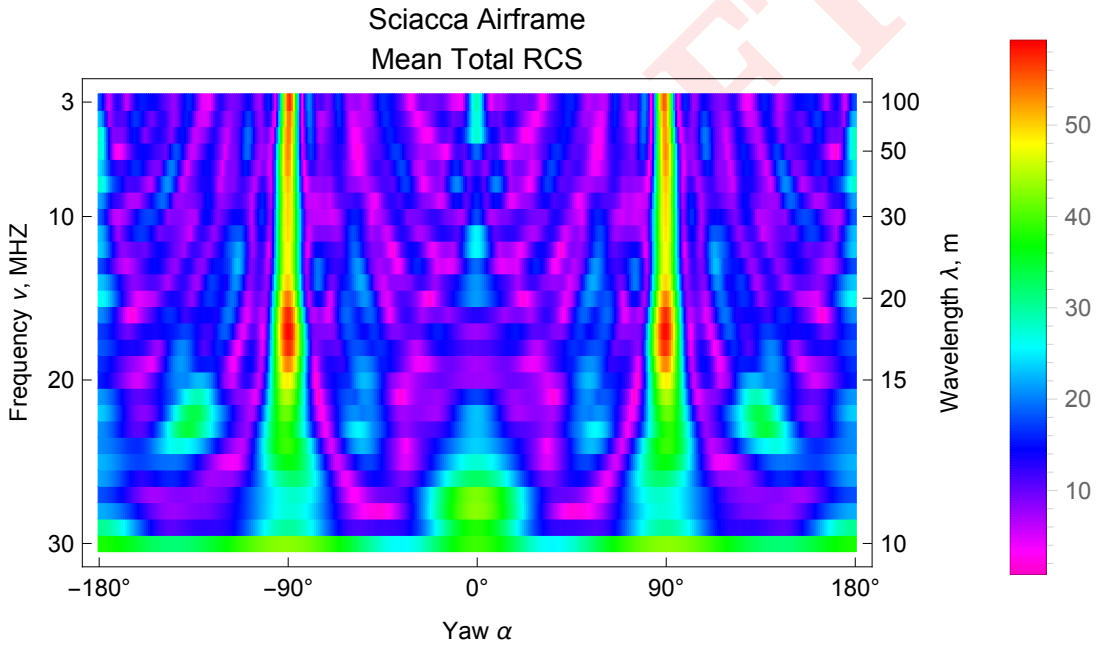

Figure 1.2: A sample calculation in Mercury MoM showing the computed value for the mean total radar cross section as a function of frequency.

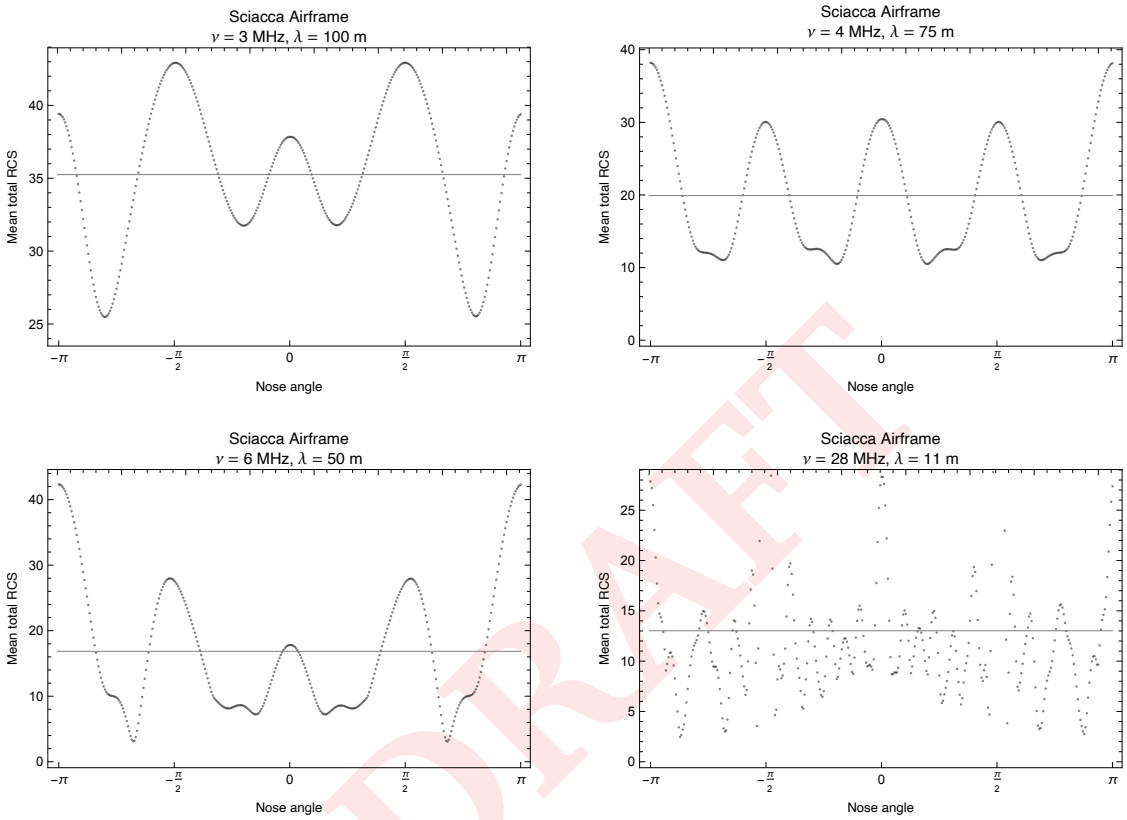

Table 1.2: A sampling of RCS computations for wavelengths of 100 m (top left), 75 m (top right), 50 m (bottom left), 11 m (bottom right). The line represents the mean value.

Current RCS	Enhanced RCS
constant	$\sigma(\alpha, \beta)$
$\sigma \in \mathbb{R}^+$	$\sigma : \mathbb{R}^2 \mapsto \mathbb{R}$

Table 2.1: In a nutshell: enhance the AFCAP Dashboard by using a richer depiction of radar cross section.

2 RCS and the AFCAP Dashboard

2.1 Current and Enhanced Capabilities of the Dashboard

Currently, the AFCAP Dashboard treats target radar cross section as a constant. If we think of this as the constant term in the Fourier expansion, then we see it is the dominant term and a first step. Subsequent steps would be to improve the expansion and encode specific information about the target interaction with the radar. The enhancement is then extending the radar cross section from a scalar to a function of the yaw and pitch angles α and β as summarized in table 2.1.

At this stage of development, the pitch angle will be kept constant at $\beta = \frac{\pi}{12}$.

Table 2.2 details the operational differences between the current RCS procedure and the procedure for an enhanced RCS. Instead of selecting from a set of constant RCS values, the user will select an asset which then has detailed RCS spectrum. To unlock the spectrum, the user need to select the operating frequency of the radar, and the pitch angle (related to the intercept angle).

	current		enhanced
1.	select target type (fly or float)	1.	select asset (A, B, ...)
2.	select RCS (2^k, $k \in \mathbb{Z}^+$)	2.	pick radar frequency in MHz, $3 \leq \nu \leq 30$
		3.	pick yaw angle $\alpha \in [-\pi, \pi]$
		4.	pitch angle is fixed at $\beta = \pi/12$

Table 2.2: AFCAP Dashboard capability for RCS.

2.2 Dashboard details

The current Dashboard presents a series of options to allow the user to specify a radar cross section. An example is shown in figure 2.1.

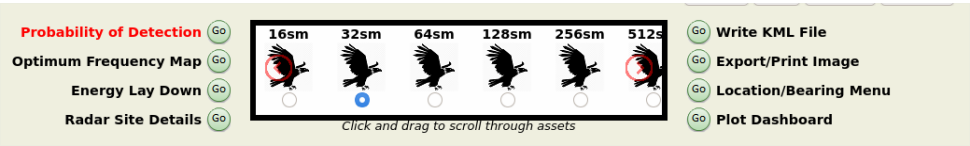

Figure 2.1: AFCAP Dashboard tool for selecting radar cross section of an airborne target.

The RCS is stored in `ConfigRegion.xml`, and the example below shows a constant radar cross section of 16 m^2:

```
<Asset>
  <Label>16sm</Label>
  <ICONImage>Bald_Eagle-sm.png</ICONImage>
  <crossSection>16</crossSection>
  <description>Aircraft</description>
  <nominalSpeed>400</nominalSpeed>
  <CIT>2.0</CIT>
</Asset>
```

The radar cross section then is used to compute the probability of detection. The beginnings of the calculation look like this:

```
from frOPCclass.js
function plotProbability (ctx, jsonObj, jsonCoord, xSection, assetCIT,
nomSpeed) {
    ...
  var xSecRadius = Math.sqrt(xSection/Math.PI)
  var sphereArea = Math.PI * xSecRadius * xSecRadius;
    ...
}
```

ϵ_0	vacuum electric permittivity	8.854×10^{-12} F m^{-1}
μ_0	vacuum magnetic permeability	1.257×10^{-7} N A^{-2}

Table 3.1: Constants used in Maxwell's equations

3 Computing the Radar Cross Section

The computation of the radar cross section is based on a simple scenario guided by Maxwell's equations. A radar illuminates the target with radar energy. The target, acting like an antenna, reradiates the energy and illuminates the radar receiver. The radar cross section is measurement of the difference between energy absorbed and energy radiated.

One form of the radar cross section equation is

$$\sigma = 4\pi r^2 \frac{S_r}{S_t} \tag{3.1}$$

where r is the distance to the target, S_t is the energy *intercepted* by the target and S_r is the energy *radiated* by the target. The result has units of area and can be compared to an ideally reflecting sphere.

The areal measure σ is computed through numerical simulation by the program Mercury MoM.

3.1 Maxwell's Equations

The mathematical foundation for the radar cross section computation is the set of Maxwell's equations. Start with two conservative fields on a simply connected domain, the electric field $\mathbf{E}\colon \mathbb{R}^3 \mapsto \mathbb{R}^3$, and the magnetic field $\mathbf{B}\colon \mathbb{R}^3 \mapsto \mathbb{R}^3$. We can relax the requirements for the electric current $\mathbf{J}\colon \mathbb{R}^3 \mapsto \mathbb{R}^3$. The differential form of Maxwell's equations in SI units is

$$\begin{array}{rclrcl} \nabla \cdot \mathbf{E} & = & \frac{\rho}{\epsilon_0} & \nabla \times \mathbf{E} & = & -\partial_t \mathbf{B} \\ \nabla \cdot \mathbf{B} & = & 0 & \nabla \times \mathbf{B} & = & \mu_0 \left(\mathbf{J} + \epsilon_0 \partial_t \mathbf{E} \right) \end{array} \tag{3.2}$$

The fundamental physical constant in SI units are given in table 3.1.

3.2 Method of Moments

There is a rich mathematical toolkit for the solution of Maxwell's equations. Mercury MoM uses the method of moments (MoM), also known as the bound-

ary element method (BEM). Maxwell's equations in integral form

$$\begin{aligned}
\nabla \cdot \mathbf{E} &= \frac{\rho}{\epsilon_0} &\Rightarrow \oint_{d\Omega} \mathbf{E} \cdot d\mathbf{S} &= \int_{\Omega} \rho dV \\
\nabla \times \mathbf{E} &= -\partial_t \mathbf{B} &\Rightarrow \oint_{d\Omega} \mathbf{B} \cdot d\mathbf{S} &= 0 \\
\nabla \cdot \mathbf{B} &= 0 &\Rightarrow \oint_{d\Sigma} \mathbf{E} \cdot d\mathbf{l} &= -\frac{d}{dt}\mathbf{B} \cdot d\mathbf{S} \\
\nabla \times \mathbf{B} &= \mu_0 \left(\mathbf{J} + \epsilon_0 \partial_t \mathbf{E}\right) &\Rightarrow \oint_{d\Sigma} \mathbf{B} \cdot d\mathbf{l} &= \mu_0 \int_{\Sigma} \left(\mathbf{J} + \epsilon_0 \frac{d}{dt}\mathbf{E}\right) \cdot d\mathbf{S}
\end{aligned} \tag{3.3}$$

The method of moments creates dense matrices which implies quadratic growth in storage and computation time as the problem scales up.

3.3 Mercury MoM Example

The power of Mercury MoM is the ability to simultaneously solve equations with millions of unknowns using a patented low rank approximation method for the linear system.

Internally, the Mercury MoM package resolves the signal emitted from the target into two complex electric fields: θ for the vertical component and ϕ for the horizontal component. As these fields are complex, they each have orthogonal real and imaginary components.

The prescription for the mean total radar cross section is taken from the Sciacca report as the average of the total field energy

$$\langle \sigma_T \rangle = \tfrac{1}{2} \left(\theta^* \theta + \theta^* \phi + \phi^* \theta + \phi^* \theta\right), \tag{3.4}$$

and is assigned areal units of squared meters m^2.

4 Fourier Expansion

4.1 Approximation Sequence

Table 4.1 presents a sequence of increasing order of Fourier approximation to a sample RCS curve ($\nu = 3$ MHz). The last graph, shows a good match to the data set using only eight numbers. The errors are quantified and compared in table 4.2.

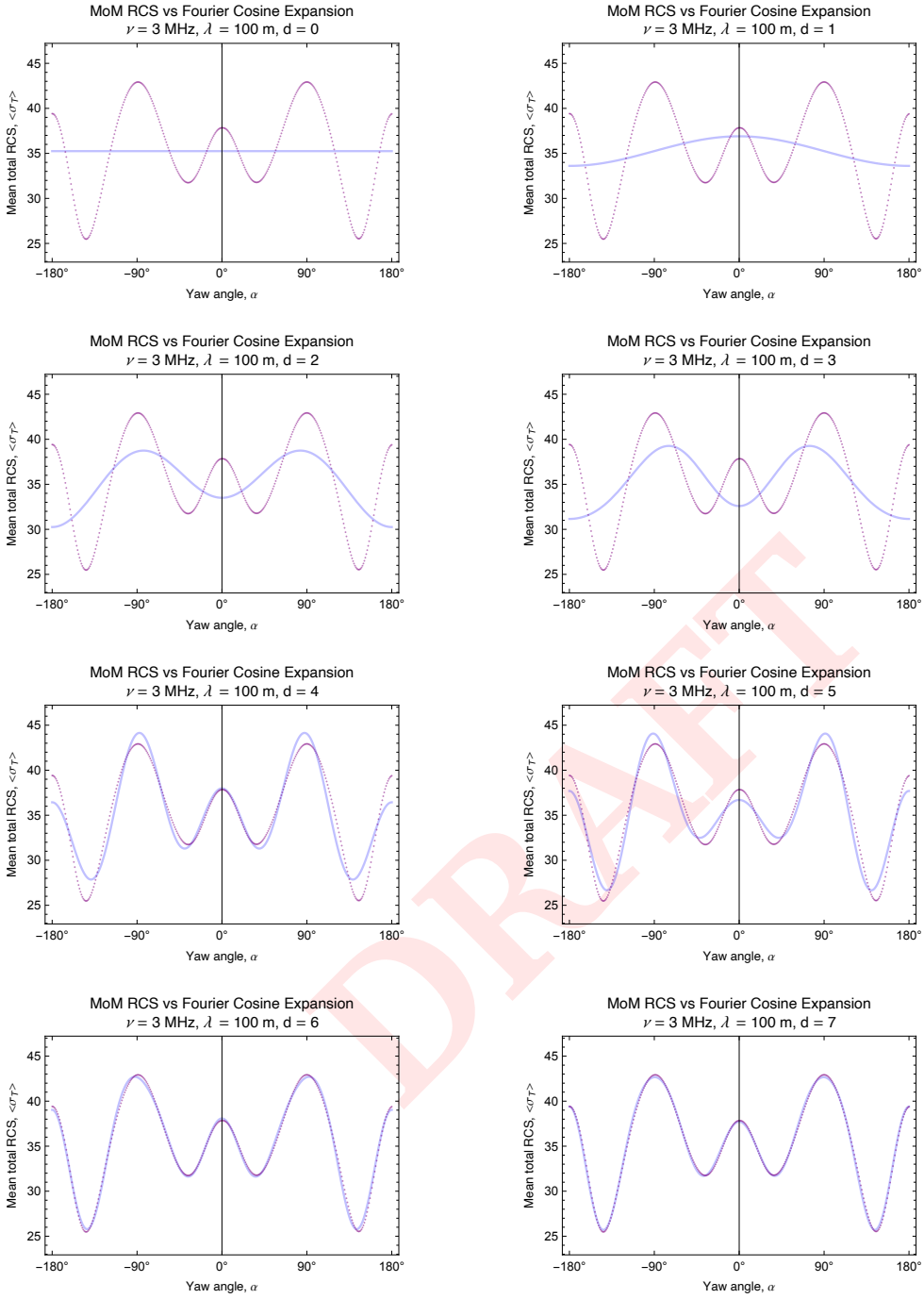

Table 4.1: Approximation sequence for an RCS measurement at $\nu = 3$ MHz. The purple dots are RCS values computed with MoM; the blue line is the trigonometric approximation.

4.2 Why Fourier?

What is the best way to approximate information in the cross sections curves shown in figure 1.2? Given that the data is periodic over the unit circle,

$$\sigma_\nu(\alpha, \beta) = \sigma_\nu(\alpha + 2\pi, \beta) \tag{4.1}$$

an obvious choice is the Fourier series. For example, a dth order approximation can be written as

$$\sigma_\nu\left(\alpha, \beta_0 = \tfrac{\pi}{12}\right) \approx \frac{a_0}{2} + \sum_{k=1}^{d} a_k \cos k\alpha + b_1 \sin k\alpha. \tag{4.2}$$

This series represents a sequence of oscillations about the mean value.

There are three powerful theoretical reasons which support this choice. The first is the convergence of the series. The Weierstrass Approximation Theorem (8.1) states that the polynomial approximation of smooth curves converges *uniformly*. That is, we can define a maximum error $\epsilon > 0$ and we are guaranteed the existence of $N \in \mathbb{Z}^+$ such that

$$\left\| \sigma_\nu(\alpha, \beta_0) - \frac{a_0}{2} - \sum_{k=1}^{N} a_k \cos k\alpha + b_k \sin k\alpha \right\|_\infty \leq \epsilon. \tag{4.3}$$

The ability to choice a maximum error is both remarkable and useful. However, the application to trigonometric polynomials, while valid, is not immediate and will be reported later.

The second reason is the Riesz–Fischer theorem, (8.2). While often cited as foundation proof that the Lebesgue space L^2 is complete, it also establishes that an infinite series whose terms converge quadratically represents an L^2 function. And so the amplitudes, the a and b values, will eventually converge at least quadratically.

The final reason is the often-overlooked fact that of all the orthogonal polynomials, only the trigonometric polynomials are topology in both the continuous topology of L^2 and and the discrete orthogonality of l^2. Having an orthogonal basis decouples the problem and can be solved mode-by–mode, obviating the need to solve a large linear system.

4.3 Orthogonality

Given non-zero integers m and n, the expression of orthogonality in L^2 can be written as

$$\begin{aligned}
\int_{-\pi}^{\pi} \sin(mx)\sin(nx)\,dx &= \pi\delta_n^m \\
\int_{-\pi}^{\pi} \cos(mx)\cos(nx)\,dx &= \pi\delta_n^m \\
\int_{-\pi}^{\pi} \cos(mx)\sin(nx)\,dx &= 0 \\
\int_{-\pi}^{\pi} \sin(mx)\,dx &= 0 \\
\int_{-\pi}^{\pi} \cos(mx)\,dx &= 0
\end{aligned} \tag{4.4}$$

where δ_n^m is the Kronecker delta tensor. To complete the toolkit to solve the linear system, recall that

$$\int_{-\pi}^{\pi} 1dx = 2\pi. \tag{4.5}$$

The linear system decouples and amplitudes for each mode can be computed independently:

$$\begin{aligned}
a_0 &= \tfrac{1}{\pi}\int_{-\pi}^{\pi} f(x)dx \\
a_k &= \tfrac{1}{\pi}\int_{-\pi}^{\pi} f(x)\cos kx dx \\
b_k &= \tfrac{1}{\pi}\int_{-\pi}^{\pi} f(x)\sin kx dx
\end{aligned} \tag{4.6}$$

where $k = 1, 2, 3, \ldots$.

4.4 Projection

Consider the low–order approximation

$$f(\varphi) \approx \frac{a_0}{2} + a_1\cos\varphi + a_2\cos 2\varphi. \tag{4.7}$$

To compute the amplitudes $a = \{a_0, a_1, a_2\}$, use Hilbert's projection theorem, which is tantamount to using the method of least squares. Multiply both

sides of the equation by $\cos j\varphi$ and integrate over the domain to isolate the contribution of a_j. For example, to isolate the component a_2,

$$\begin{aligned}\int_{-\pi}^{\pi} f(\varphi)\cos 2\varphi d\varphi &\approx \int_{-\pi}^{\pi}\left(\frac{a_0}{2}+a_1\cos\varphi+a_2\cos 2\varphi\right)\cos 2\varphi d\varphi. \\ &= a_2\int_{-\pi}^{\pi}\cos^2 2\varphi d\varphi.\end{aligned} \tag{4.8}$$

The general formula is

$$a_k = \frac{1}{\pi}\int_{-\pi}^{\pi} f(\varphi)\cos k\varphi d\varphi, \quad k = 1, 2, 3, \ldots \tag{4.9}$$

Because the basis functions are orthogonal, the modes are decoupled and the amplitudes can be computed independently.

4.5 Discrete Topology

The continuum formulation in L^2 is useful for understanding the critical components of the theory and makes a natural starting point for discussing the discrete topology of l^2. The moment we discretize the problem in a computer code, we switch from the continuum to a discrete space. Out of all the known orthogonal polynomials, only two are orthogonal in both L^2 and l^2, and these are the sine and cosine functions.

However, because of sampling mesh that was used in Mercury MoM, the data vectors are *not* orthogonal and the amplitudes are found by solving a dense linear system.

4.6 Special Case: The Mean

The Fourier series resolves a function into successively higher oscillations about a constant value. This constant value is the mean, a least squares solution, and, a valuable bellwether. If the system is orthogonal, the the $a_0/2$ term will be the mean. But if the mesh precludes orthogonality, the a_0 will fluctuate in value for distinct fits.

4.6.1 The Method of Least Squares

Consider the least squares problem of representing a sequence of values by a single number. Intuitively, the number is the average. But it is also a solution to the least squares problem. Start by defining the sum of the squares of the

residual errors,

$$r^2 = \sum_{k=1}^{m} \left(\sigma\left(\alpha_k, \beta_0\right) - \mu\right)^2, \tag{4.10}$$

and minimize this quantity with respect to the lone parameter, auspiciously named μ. Using the calculus, the roots of the first derivative are defined as:[2]

$$D_\mu r^2 = -2 \sum_{k=1}^{m} \left(\sigma\left(\alpha_k, \beta_0\right) - \mu\right) = 0. \tag{4.11}$$

Solving (4.11) for μ produces

$$\mu = m^{-1} \sum_{k=1}^{m} \sigma\left(\alpha_k, \beta_0\right). \tag{4.12}$$

The least squares solution for the parameter μ is simply the average of the data, the arithmetic mean. Formally, we may think of the mean as the first and dominant term in the Fourier decomposition.

4.6.2 Moving from continuous topology to discrete topology

The continuum formulation translates to discrete spaces using the idea of the integral as a Riemann sum:

$$\int_{-\pi}^{\pi} \cos\left(j\alpha_k\right) d\alpha \quad \Rightarrow \quad \sum_{k=1}^{m} \cos\left(j\alpha_k\right) \Delta_k. \tag{4.13}$$

Here Δ_k, the interval length, corresponds to the Riemann integration measure $d\alpha$. A basic result from the calculus is that the average $\langle f\left(x\right)\rangle$ of an integrable function over a finite, ordered interval $G = [a, b]$ is

$$\langle f\left(x\right)\rangle = \frac{\int_b^a f(x)dx}{b-a}, \tag{4.14}$$

where the interval length $L = b - a$.

Next, consider the discretized interval $g = [a, b]$ The connection to the discrete case is clear with the realization that the Mercury MoM results are spaced at regular intervals of 1°, that is,

$$\Delta_k = \Delta.$$

[2]The root is guaranteed to be a minimum as the set of least squares minimizers is a convex set. See theorem 8.3.

Then the interval length is

$$L = \sum_{k=1}^{m} \Delta_k = \sum_{k=1}^{m} \Delta = m\Delta. \tag{4.15}$$

The average function value is in the same form as the least squares solution in (4.12):

$$\begin{aligned} \langle f(x) \rangle_G &= \frac{\int_b^a f(x)dx}{L}, \\ \langle f(x) \rangle_g &= \frac{\sum_{k=1}^{m} f(x_k)\Delta}{m\Delta} = m^{-1} \sum_{k=1}^{m} f(x_k). \end{aligned} \tag{4.16}$$

4.7 Linear Independence

In an orthogonal system, the frequency modes decouple allowing amplitudes for each frequency to be computed individually. And while the sampling locations (mesh) can be specified to enforce orthogonality, it was not. Without recourse to orthogonality, the solution relies instead upon linear independence.

Equation (4.7) implies a sequence of m equations:

$$\begin{array}{ccccccc} \frac{a_0}{2} & + & a_1 \cos\alpha_1 & + & a_2 \cos 2\alpha_1 & = & \sigma(\alpha_1, \beta_0) \\ \vdots & & \vdots & & \vdots & & \vdots \\ \frac{a_0}{2} & + & a_1 \cos\alpha_m & + & a_2 \cos 2\alpha_m & = & \sigma(\alpha_m, \beta_0) \end{array} \tag{4.17}$$

4.7.1 Forming the linear system

First pose the linear system:

$$\begin{array}{ccc} \mathbf{A} & a & = & \Sigma \\ \begin{bmatrix} 1 & \cos\alpha_1 & \cos 2\alpha_1 \\ \vdots & \vdots & \vdots \\ 1 & \cos\alpha_m & \cos 2\alpha_m \end{bmatrix} & \begin{bmatrix} a_0 \\ a_1 \\ a_2 \end{bmatrix} & = & \begin{bmatrix} \sigma(\alpha_1, \beta_0) \\ \vdots \\ \sigma(\alpha_m, \beta_0) \end{bmatrix}. \end{array} \tag{4.18}$$

In the continuum, we can use projection ...

4.7.2 Posing the normal equations

For both L^2 and l^2 formulations, pose the normal equations:

$$\mathbf{A}^* \mathbf{A} a = \mathbf{A}^* \Sigma \tag{4.19}$$

where the product matrices are

$$\begin{aligned}
\mathbf{A}^*\mathbf{A} &= \begin{bmatrix} \mathbf{1}\cdot\mathbf{1} & \mathbf{1}\cdot(\cos\alpha) & \mathbf{1}\cdot(\cos 2\alpha) \\ (\cos\alpha)\cdot\mathbf{1} & (\cos\alpha)\cdot(\cos\alpha) & (\cos\alpha)\cdot(\cos 2\alpha) \\ (\cos 2\alpha)\cdot\mathbf{1} & (\cos 2\alpha)\cdot(\cos\alpha) & (\cos 2\alpha)\cdot(\cos 2\alpha) \end{bmatrix}, \\
\mathbf{A}^*\Sigma &= \begin{bmatrix} \mathbf{1}\cdot\sigma(\alpha,\beta_0) \\ (\cos\alpha)\cdot\sigma(\alpha,\beta_0) \\ (\cos 2\alpha)\cdot\sigma(\alpha,\beta_0) \end{bmatrix}.
\end{aligned} \tag{4.20}$$

The measurement vectors are, for example,

$$(\cos\alpha)^T = (\cos\alpha_1, \cos\alpha_2, \ldots, \cos\alpha_m), \tag{4.21}$$

while the data vector is

$$\sigma(\alpha,\beta_0)^T = (\sigma(\alpha_1,\beta_0), \sigma(\alpha_2,\beta_0), \cdots, \sigma(\alpha_m,\beta_0)), \tag{4.22}$$

and the vector of unit entries is

$$\mathbf{1}^T = \underbrace{(1,1,\ldots,1)}_{m \text{ instances}}. \tag{4.23}$$

Theorem 8.4 establishes that if a solution to the normal equations exist, it will be equivalent to the least squares solution.

4.8 Solution via the normal equations

If the mesh supported orthogonality, the off–diagonal terms would be zero, and the system would then be decoupled. But this was not the case of the data generated for the Sciacca airframe. The solution to the normal equations is

$$a = (\mathbf{A}^*\mathbf{A})^{-1}\mathbf{A}^*\Sigma. \tag{4.24}$$

4.9 Error propagation

A great, and, too–often overlooked, power of the method of least squares is the quantitative error factors. In addition to computing the amplitudes, we may also propagate the measurement errors through the computation chain to determine how precisely the amplitudes are known. The general formula for the ϵ_k, the error in the parameter a_k, is

$$\epsilon_k = \sqrt{\frac{r\cdot r}{m-n}(\mathbf{A}^*\mathbf{A})^{-1}_{kk}}. \tag{4.25}$$

The error depends upon the sum of the squares of the residual errors $(r \cdot r)$, the difference between the number of samples (m), and, the number of fit parameters (n) and the kth diagonal term of the inverse of the product matrix $\mathbf{A}^*\mathbf{A}$.

Figure 4.1 shows the value of the plotting error bars. Results are shown for a fit of order $d = 25$. We can instantly see that the higher order modes, a_{14} and beyond, are statistically indistinguishable from zero. Computer time spent on their computation has been wasted.

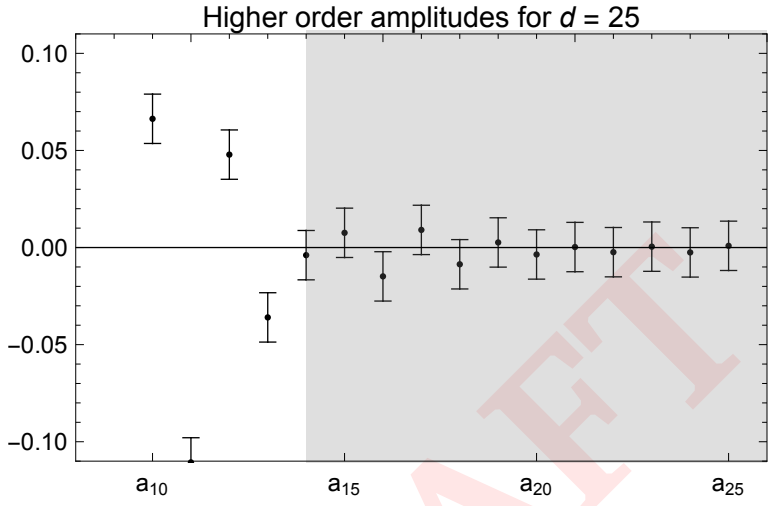

Figure 4.1: A look at the amplitudes for a fit of order $d = 25$ shows that the amplitudes a_{14} and higher are statistically indistinguishable from zero. They make no appreciable contribution to the quality of decomposition.

4.10 Quality of Fit

How many nodes are needed to capture the information content of a cross section curve, such as the four shown in table 1.2? Ultimately the amplitudes will reach quadratic or sub–quadratic convergence which rapidly diminishes contributions from higher frequencies. However, numerical errors intrude which blur the resolution needed to resolve incremental improvements. There are four common ways to evaluate the quality of fit.

1. Dominance of modes,
2. Maximum error, $\|r\|_\infty$ (the norm of the Weierstrass theorem)

3. Total error, $\|r\|_2^2$ (least squares)
4. error ratio, a_k/ϵ_k (signal–to–noise)

The plots in table 4.2 analyze the cross section at $\nu = 3$ MHz for orders $d = 0, 1, 2 \ldots 25$. The cross-hairs show the values used for $d = 7$, the final figure for the Fourier decomposition sequence in table 4.1.

4.10.1 Dominance of modes

Fourier decomposition excels at identifying the strength of the contributions of each term. In the example, the plot showing the strength of contribution for each term in figure 5.2 will show strong dominance for the mean, and dominance for the 4α and 2α terms.

4.10.2 Maximum error

The promise of the Weierstrass theorem is uniform convergence to an arbitrary error level, a suggestion to evaluate $\|r\|_\infty$. However, in the presence of numerical errors in the measurements, the error will typically plateau, or perhaps even exhibit a distinct minimum.

4.10.3 Total error

The total error is the quantity minimized in the least squares solution. In the ideal case, this would fall to zero. In following example, the two error norms, $\|r\|_\infty$ and $\|r\|_2$, tell nearly identical stories: computations above $d = 10$ add little to quality of the fit.

4.10.4 Signal to noise

The error bars provide a measure of signal to noise. As a rapid way to compare modes across the decomposition sequence for $d = 0$ to $d = 25$, the plot considers the error in the highest mode. The gray shading in the plot is the region where the noise is stronger that the signal.

5 Numeric Example

5.1 Data

A specific example will make the theoretical ideas concrete. The data source, the file `PTW.4112.txt` is described in more detail in table 5.1. Note the precise

metric	cumulative plot
$\|r\|_2^2$	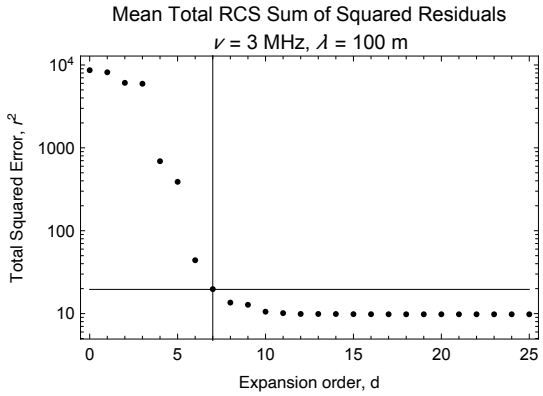
$\|r\|_\infty$	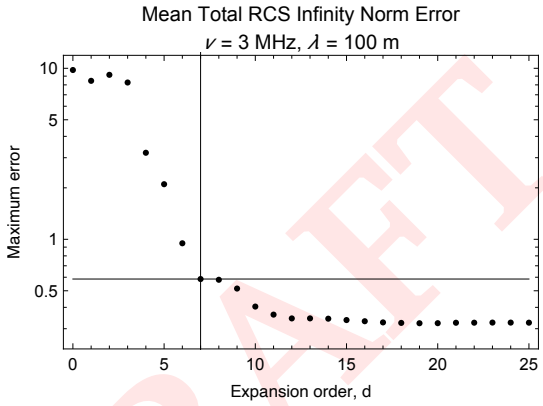
$\frac{a_{d_{max}}}{\epsilon_{d_{max}}}$	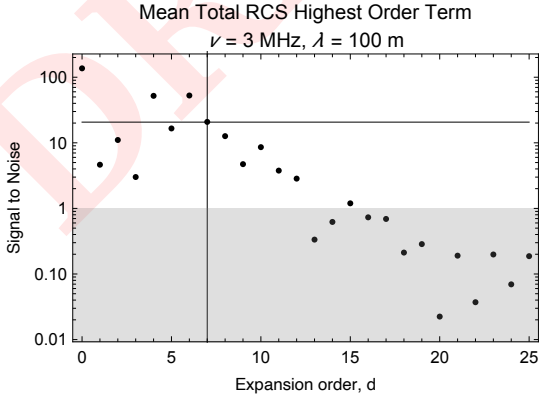

Table 4.2: Graphical comparison of criteria for truncating the Fourier expansion. The crossed lines mark values at $d = 7$, the final plot in table 4.1.

inpute file	`PTW.4112.txt`
mean value	35.248 773 556 863 84
frequency	$\nu = 3$ MHz
wavelength	$\lambda = 100$ m
angular sampling range	$0° - 360°$
angular sampling interval	$1°$

Table 5.1: The data file from Mercury MoM used for this example.

computation of the mean value. The data is plotted in figure 5.2 and shows the output from Mercury MoM: an RCS value for each degree of yaw, α.

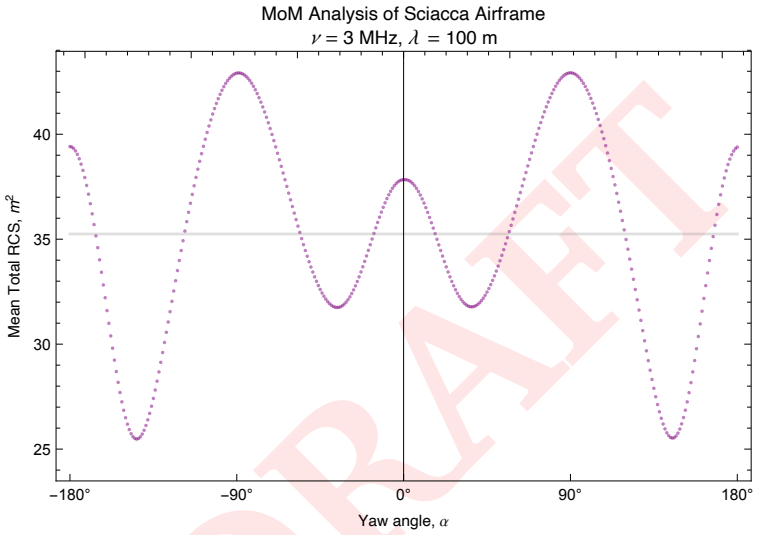

Figure 5.1: Sample data set for $\nu = 3$ MHz. The output from MoM (purple dots) is shown against the mean value (gray line).

5.2 Results

5.2.1 Approximation sequence

For comparison, an a sequence of decompositions was performed to provide a sketch of how the approximation improves.

d	a_0	a_1	a_2	a_3	a_4	a_5	a_6	a_7
0	35.2488							
1	35.2533	1.64293						
2	35.2626	1.62429	−3.38356					
3	35.2601	1.62928	−3.38855	−0.912138				
4	35.2455	1.65863	−3.41790	−0.882795	5.38447			
5	35.2420	1.66561	−3.42488	−0.875809	5.37749	−1.28893		
6	35.2383	1.67306	−3.43233	−0.868366	5.37004	−1.28148	1.38079	
7	35.2373	1.67502	−3.43429	−0.866400	5.36808	−1.27952	1.37883	−0.366535

Table 5.2: Amplitudes for the approximation sequence shown in table 4.1. In the ideal case the amplitudes a would have constant values independent of the order. For example, note the variation in the a_0 term.

5.2.2 Specific solution

For a specific solution, the decomposition for $d = 7$ was chosen. (This is the final line in table 5.2.) The most dominant modes are a_0, the mean, a_4, corresponding to $\cos 4\alpha$, and, finally, a_2, corresponding to $\cos 2\alpha$.

The functional representation of the RCS in terms of the yaw angle α is

$$\begin{aligned}\sigma(\alpha) \approx\, & 35.2373 + 1.67502\cos\alpha - 3.43429\cos 2\alpha \\ & - 0.8664\cos 3\alpha + 5.36808\cos 4\alpha - 1.27952\cos 5\alpha \\ & + 1.37883\cos 6\alpha - 0.366535\cos 7\alpha,\end{aligned} \tag{5.1}$$

and this is the function to use with the AFCAP Dashboard.

5.3 Fauxthogonality

Due to problems with the mesh having a supernumerary point, the orthogonality relationship for the cosine vectors is destroyed, and we must solve a dense linear system.

5.3.1 Dense linear system

Using the MoM data, the product matrix is not diagonal; off–diagonal terms have unit magnitude. Of course, you can't solve this linear system by pretend-

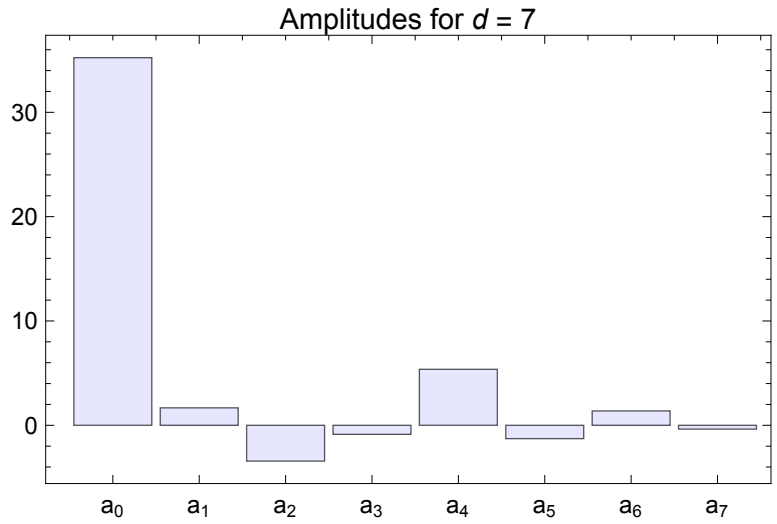

Figure 5.2: The amplitudes for the $d = 7$ decomposition, the final line of table 5.2.

ing the off–diagonal terms are zero. It is a dense linear system whose

$$\mathbf{A}^*\mathbf{A} = \begin{bmatrix} 361 & -1 & 1 & -1 & 1 & -1 & 1 & -1 \\ -1 & 181 & -1 & 1 & -1 & 1 & -1 & 1 \\ 1 & -1 & 181 & -1 & 1 & -1 & 1 & -1 \\ -1 & 1 & -1 & 181 & -1 & 1 & -1 & 1 \\ 1 & -1 & 1 & -1 & 181 & -1 & 1 & -1 \\ -1 & 1 & -1 & 1 & -1 & 181 & -1 & 1 \\ 1 & -1 & 1 & -1 & 1 & -1 & 181 & -1 \\ -1 & 1 & -1 & 1 & -1 & 1 & -1 & 181 \end{bmatrix} \tag{5.2}$$

This matrix has full rank, and the inverse can be computed directly and the result is detailed in the final line of table 5.2.

$$(\mathbf{A}^*\mathbf{A})^{-1} = \frac{1}{67500} \begin{bmatrix} 187 & 1 & -1 & 1 & -1 & 1 & -1 & 1 \\ 1 & 373 & 2 & -2 & 2 & -2 & 2 & -2 \\ -1 & 2 & 373 & 2 & -2 & 2 & -2 & 2 \\ 1 & -2 & 2 & 373 & 2 & -2 & 2 & -2 \\ -1 & 2 & -2 & 2 & 373 & 2 & -2 & 2 \\ 1 & -2 & 2 & -2 & 2 & 373 & 2 & -2 \\ -1 & 2 & -2 & 2 & -2 & 2 & 373 & 2 \\ 1 & -2 & 2 & -2 & 2 & -2 & 2 & 373 \end{bmatrix} \tag{5.3}$$

k	$\cos k\alpha$	amplitude
0	1	35.237 277 592 785 375
1	$\cos\alpha$	1.675 022 046 154 634 1
2	$\cos 2\alpha$	−3.434 292 043 875 646
3	$\cos 3\alpha$	−0.866 400 204 593 953 2
4	$\cos 4\alpha$	5.368 077 161 998 904 5
5	$\cos 5\alpha$	−1.279 517 980 533 678 3
6	$\cos 6\alpha$	1.378 826 401 472 061 7
7	$\cos 7\alpha$	−0.366 535 373 755 586 9

Table 6.1: The Fourier amplitudes for the data shown in figure 5.2 and represented in (5.1).

5.3.2 Decoupled linear system

If the mesh is corrected, the orthogonality of the vectors will manifest with a decoupled linear system: terms can be computed mode–by–mode.

$$\mathbf{A}^*\mathbf{A} = \begin{bmatrix} 360 & 0 & 0 & 0 & 0 & 0 & 0 & 0 \\ 0 & 180 & 0 & 0 & 0 & 0 & 0 & 0 \\ 0 & 0 & 180 & 0 & 0 & 0 & 0 & 0 \\ 0 & 0 & 0 & 180 & 0 & 0 & 0 & 0 \\ 0 & 0 & 0 & 0 & 180 & 0 & 0 & 0 \\ 0 & 0 & 0 & 0 & 0 & 180 & 0 & 0 \\ 0 & 0 & 0 & 0 & 0 & 0 & 180 & 0 \\ 0 & 0 & 0 & 0 & 0 & 0 & 0 & 180 \end{bmatrix} \tag{5.4}$$

6 Validation Exercise

The previous section presented results for a seventh order decomposition to connect the theory to the computation. The goal of this section is to extend the example and provide data suitable for code validation. That is, to be able to check a computer code to full double precision.

The inputs for the amplitudes are quoted to full double precision in table 6.1.

Given the amplitudes at full precision, it is straightforward to compute the

results for special cases.

α	α°	$\sigma(\alpha)$
0	0°	37.712 457 599 652 11
$\pi/4$	45°	32.311 833 530 507 33
$\pi/2$	90°	42.660 820 397 187 86
$3\pi/4$	135°	27.426 567 331 065 61
π	180°	39.387 320 625 109 275
$3\pi/4$	225°	27.426 567 331 065 61
$3\pi/2$	270°	42.660 820 397 187 86
$7\pi/4$	315°	32.311 833 530 507 33
2π	360°	37.712 457 599 652 11

7 References

1. Fourier Series
   (a) Wolfram MathWorld Fourier Series
   (b) Wikipedia Fourier series
   (c) SOS Math Fourier Series: Basic Results
2. Maxwell's Equations
   (a) http://www.maxwells-equations.com
   (b) Wikipedia Maxwell's equations
   (c) Brilliant.org Maxwell's Equations
3. Method of Moments
   (a) MIT OpenCourseWare The Method of Moments in Electromagnetics
   (b) Wikipedia Method of moments element method
   (c) EMAG Technologies Basic Principles of The Method of Moments
   (d) ResearchGate A Tutorial on the Method of Moments
4. Radar Cross Section
   (a) Wikipedia Radar cross-section
   (b) Microwaves101.com Radar Cross-Section Physics
   (c) GlobalSecurity.org Radar Cross Section (RCS)
   (d) Introduction to Radar Systems Target Radar Cross Section

8 Theorems and Proofs

Theorem 8.1 (Weierstrass Approximation Theorem)**.** *Polynomials are dense in the space of continuous functions with respect to the uniform norm.*

Proof. See, for example, x, y, z. □

Theorem 8.2 (Riesz-Fischer)**.** *Let $\{\phi_n\}$ be an orthonormal sequence of functions on Ω and suppose $\sum |a_n|^2$ converges. Denote the partial sum as*

$$s_\tau = a_0\phi_0 + a_1\phi_1 + \cdots + a_\tau\phi_\tau.$$

There exists a function $F \in L^2$ such that $\{s_\tau\}$ converges to F in L^2, and such that

$$F = \sum_{k=0}^{\infty} a_k\phi_k,$$

almost everywhere.

Proof. See, for example, x, y, z. □

Theorem 8.3 (Convexity of least squares minimizers)**.** *Given a matrix $\mathbf{A} \in \mathbb{C}_\rho^{m\times n}$ with rank $(\rho \leq n)$, and a data vector $b \in \mathbb{C}^m$, then χ, the set of least squares minimizers,*

$$\chi = \underset{x\in\mathbb{C}^n}{\arg\min} \left\|\mathbf{A}\,x - b\right\|_2,$$

is a convex set.

Proof. Take two elements $x_1, x_2 \in \chi$ and a variation parameter $\lambda \in [0, 1]$. Establish that the linear combination is also in the set of minimizers:

$$\lambda x_1 + (1-\lambda)\,x_2 \in \chi \tag{8.1}$$

Use the fact that $b = \lambda b + (1-\lambda)b$ and triangle inequality to show

$$\left\|\mathbf{A}\left(\lambda x_1 + (1-\lambda)\,x_2\right) - b\right\|_2^2 \leq \lambda\left\|\mathbf{A}\,x_1 - b\right\|_2^2 + (1-\lambda)\left\|\mathbf{A}\,x_2 - b\right\|_2^2 \tag{8.2}$$

Because the x variables are minimizers, the norms achieve the minimum value (least total squared error) t^2.

$$\lambda\left\|\mathbf{A}\,x_1 - b\right\|_2^2 + (1-\lambda)\left\|\mathbf{A}\,x_2 - b\right\|_2^2 = \lambda t^2 + (1-\lambda)\,t^2 = t^2 \tag{8.3}$$

From which we conclude

$$\left\|\mathbf{A}\left(\lambda x_1 + (1-\lambda)\,x_2\right) - b\right\|_2^2 = t^2,\ \forall\lambda \in [0,1] \tag{8.4}$$

thereby establishing the premise in equation (8.2). □

Theorem 8.4 (Equivalence of solutions)**.** *If x_N, a solution to normal equations exists, it must be equal to the least squares solution x_{LS}:*

$$x_{LS} = x_N.$$

Proof. By construction, the least squares minimizers

$$x_{LS} = \arg\min_{x \in \mathbb{C}^n} \|\mathbf{A}\, x - b\|_2\,, \tag{8.5}$$

define the least total error,

$$t^2 = \|\mathbf{A}\, x_{LS} - b\|_2^2\,. \tag{8.6}$$

Using the last fact and the Art of the Propitious Zero ($\mathbf{A}x_N - \mathbf{A}x_N = \mathbf{0}$) to introduce x_N thereby crafting one equation with both x_{LS} and x_N.

$$\begin{aligned} t^2 &= \|\mathbf{A}\, x_{LS} - b\|_2^2 \\ &= \|\mathbf{A}\, x_{LS} + (\mathbf{A}x_N - \mathbf{A}x_N) - b\|_2^2 = \|\mathbf{A}\,(x_{LS} - x_N) + \mathbf{A}x_N - b\|_2^2\,. \end{aligned}$$

By Pythagoras,

$$\begin{aligned} t^2 = &\|\mathbf{A}\,(x_{LS} - x_N)\|_2^2 + \|\mathbf{A}x_N - b\|_2^2 \\ &+ (\mathbf{A}\,(x_{LS} - x_N))^*\,(\mathbf{A}x_N - b) + (\mathbf{A}x_N - b)^*\,(\mathbf{A}\,(x_{LS} - x_N)) \end{aligned}$$

The first cross term vanishes because of condition (**??**):

$$(\mathbf{A}\,(x_{LS} - x_N))^*\,(\mathbf{A}x_N - b) = (x_{LS} - x_N)^*\,\mathbf{A}^*\,(\mathbf{A}x_N - b) = \mathbf{0}.$$

Because $\mathbf{0}^* = \mathbf{0}$, showing that the conjugate of the second cross term is $\mathbf{0}$ implies that the term itself is $\mathbf{0}$:

$$((\mathbf{A}x_N - b)^*\,\mathbf{A}\,(x_{LS} - x_N))^* = (x_{LS} - x_N)^*\,\mathbf{A}^*\,(\mathbf{A}x_N - b) = \mathbf{0}^* = \mathbf{0}$$

The least total squared error reduces to

$$t^2 = \|\mathbf{A}x_N - b\|_2^2 + \|\mathbf{A}\,(x_{LS} - x_N)\|_2^2$$

Argue that the right–hand side is the sum of two non-negative numbers. This constrains $\|\mathbf{A}x_N - b\|_2^2$ to the extremal value of t^2, which implies an equivalence between x_{LS} and x_N via equation (8.5). But this is not an equality, as, for example, x_N may have differing null space contributions. The desired equality follows from the second term

$$\|\mathbf{A}\,(x_{LS} - x_N)\|_2^2 = \mathbf{0} \qquad \Longrightarrow \qquad x_{LS} - x_N = \mathbf{0}.$$

Therefore, we must have

$$x_{LS} = x_N.$$

□